Characterisation of low-Reynolds number flow through an orifice: CFD results vs. laboratory data

Nuno M. C. Martins, Dídia I. C. Covas, Silvia Meniconi, Caterina Capponi and Bruno Brunone

ABSTRACT

Pressurised pipe systems transport fluids daily over long distances and sediment deposits are responsible for narrowing the cross-sectional area of the pipe. This reduces the carrying capacity in gravity pipes and increases the energy consumption in rising mains. As partial blockages do not give rise to any external evidence, they are considered the most insidious fault occurring in pipe systems. Thus, the refinement of reliable techniques for detecting partial blockages at an early stage is of great interest to water utilities. This paper presents a computational fluid dynamics (CFD)-based analysis of the steady-state flow through a sharp-edged orifice which corresponds to the most straightforward partial blockage feature in a pipe. The main motivation is the fact that the interaction between pressure waves and a partial blockage – on which Transient Test-Based Techniques for fault detection are based – is strongly influenced by the pre-transient conditions at the partial blockage. The refined CFD model has been validated by considering experimental data selected from the literature. The comparison of obtained results demonstrates good performance of the numerical model. This authorised exploring in detail the features of the flow through the orifice as a necessary premise to its use within the successive transient analysis.

Key words | CFD, low-Reynolds number flow, partial blockage, pipes, sharp-edge orifice

HIGHLIGHTS

- A comprehensive analysis of the low-Reynolds number flow through a sharp-edged orifice (partial blockage) is provided by computational fluid dynamics (CFD).
- The successful comparison of CFD with reference papers demonstrates that the model accurately describes the laminar flow through an orifice in steady-state conditions.
- The obtained results can be further used for the transient analysis of the interaction between a pressure wave and the obstacle.

Nuno M. C. Martins (corresponding author)
Dídia I. C. Covas
CERIS, Instituto Superior Técnico,
Universidade de Lisboa,
Lisboa,
Portugal
E-mail: *nunomiguelmartins@tecnico.ulisboa.pt*

Silvia Meniconi
Caterina Capponi
Bruno Brunone
Department of Civil and Environmental Engineering,
The University of Perugia,
Perugia,
Italy

doi: 10.2166/hydro.2021.101

INTRODUCTION

Fluids, such as water, refined and crude oil, are transported daily by means of pressurised pipe systems over long distances within geographical boundaries of countries or beyond. Pipeline deterioration and defects, such as leaks and partial blockages, are a frequent problem causing resource and economic losses (Ferrante *et al.* 2014). Blockages result from the combination of particles transported by the fluid, that are deposited, and the biofilm growth in the pipe inner walls due to physical, chemical and biological processes (Jing *et al.* 2018). Such processes result in the narrowing of the cross-section of the pipe in localised zones (Figure 1). In addition, if not detected at an early stage, the partial blockage protrudes transversely and extends longitudinally, which is why many water managers consider it as the most insidious fault that can affect pipeline systems. Another possible cause of a partial blockage is the air pocket accumulation at high points of pipelines with an undulating profile (e.g., Pozos-Estrada 2018).

The narrowing of the pipe cross-section due to the sediment deposit causes substantial impacts on the supply performance and operating costs of the system. In fact, partial blockages increase the head losses and, consequently, reduce the transport capacity of gravity systems and the energy consumption in rising mains. Partial blockages deteriorate water quality by promoting the survival of different food sources that serve microorganisms by simplifying their interaction (Meniconi *et al.* 2016) and, at an advanced stage, can lead to pipe rupture (Badillo-Olvera *et al.* 2019). Moreover, deposits create obstructions not only in pipes but also in the devices, such as control valves, filters and consumer taps. A similar process may occur in the cardiovascular system in which partial blockages result from the plaque formation, with potential severe effects for patients, such as stroke and heart attacks (Quarteroni *et al.* 2017).

As there is no external evidence of the reduction in the pipe cross-section, direct methods, such as visual inspection or noise measurement, as for leaks (Beck *et al.* 2018), do not allow locating a partial blockage nor assessing its severity (i.e., the ratio between the opening area and the pipe cross-section area) and extension (i.e., the length along the pipe). For these reasons, the detection and characterisation of partial blockages are of paramount importance from the pipe system management.

Conventional practices to characterise a partial blockage are based on measurements and inspections. The former approach demands a distributed set of pressure sensors, flow meters and valve sensors, highly time-consuming and expensive (Chaudhry 2014). On the contrary, the latter approach demands video inspections or ultrasonic testing through a significant part of the pipe system (Mohapatra *et al.* 2006) using semi-autonomous surveillance (Gooch *et al.* 1996) or Doppler guidewire, as for detecting stenosis in the human cardiovascular system (Bach & Kern 1997).

Based on the inspection method, Rogers (1995) developed an axial strain-sensing element to measure the blockage-induced strain variation of the pipe wall. However, this method was tested only on a subsea pipeline, and no tests have been carried out on buried pipes yet. Moreover, this procedure is time-consuming and very expensive since it requires a remote-operated vehicle to install and recover the sensing element positioned on the outer wall of the

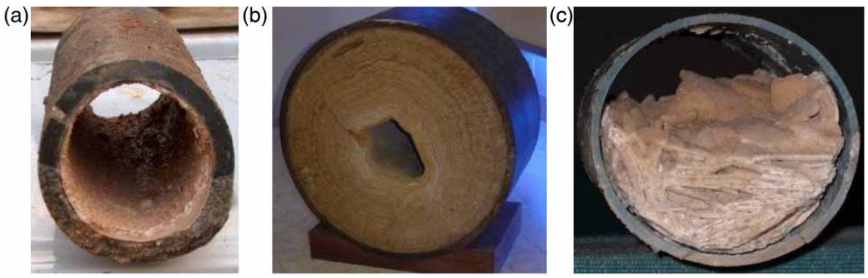

Figure 1 | Pipe cross-section narrowing due to partial blockage features for metallic pipes: (a) and (b) diameter decrease caused by the regular deposit of sediment on the inner walls; for polymeric pipes: (c) accumulation on the lower part of the pipe section of material detached from the walls (Alegre & Covas 2010).

pipe. The acoustic pulse reflectometry method is widely used and has been proved to be suitable to detect and characterise blockages. As an example, the method proposed in Qunli & Fricke (1989) and Qunli (1994), based on the theoretical and experimental analysis of eigenfrequency shifts inherent to the acoustical signals, provides enough information for evaluating the severity of the blockage.

A different approach for detecting partial blockages (Massari *et al.* 2014), as well as other defects (Duan *et al.* 2016) – such as leaks (Soares *et al.* 2011; Meniconi *et al.* 2015; Duan 2017; Li *et al.* 2020), pipe wall deteriorations (Gong *et al.* 2014), illegal branches (Meniconi *et al.* 2011c) and air pockets (Ferreira *et al.* 2020) – is the one based on carrying out safe fast transient tests, characterised by the generation of a small but sharp pressure wave (Meniconi *et al.* 2011b).

Within the Transient Test-Based Techniques (TTBTs), changes in the transient response due to the defect allow detecting its location and characteristics. With respect to the defect-free pipe, partial blockages affect the transient response in both the short and long term. Precisely, they give rise to a positive reflected pressure wave in the system first characteristic time (Contractor 1965) and increase the successive damping of the pressure peaks (Meniconi *et al.* 2012b). Moreover, for a given severity, discrete blockages (e.g., orifices and partially closed in-line valves) exhibit a quite different behaviour with respect to the extended ones (i.e., pipe branches with a narrowed cross-section) (Meniconi *et al.* 2016). Precisely, discrete partial blockages give rise to a distinct positive wave, whereas the extended ones generate a sort of bell-shaped pressure rise whose size depends on the blockage extension (Meniconi *et al.* 2012a). The importance of such features increases with the severity of the blockage. Precisely, the larger the pre-transient local head loss through a discrete partial blockage, ΔH, the larger the reflected pressure wave that is about a half of ΔH (Contractor 1965; Meniconi *et al.* 2011a).

However, notwithstanding such clear fingerprints of partial blockages in the transient pressure traces, the 1D approach allows detecting reliably only the location. On the contrary, the evaluation of the severity of partial blockages is a challenging task. In fact, several innovative methods have been proposed – e.g., the area reconstruction method (Zouari *et al.* 2020) and the one using the Bragg resonance condition (Louati *et al.* 2017) – to improve the TTBT's performance.

Thus, in the writers' opinion, within TTBTs, a decisive improvement could be achieved by deepening the insight of the mechanisms of interaction between a pressure wave and a partial blockage. In such a context, 1D models look inappropriate as they cannot include more detailed information than the local head loss through the partial blockage. On the contrary, to take into account the flow field characteristics, both upstream and downstream of the partial blockage, more complete numerical models must be used. In this regard, a possible option is refining a reliable computational fluid dynamics (CFD) model to simulate the behaviour of a partial blockage. In fact, the high flexibility and accuracy in simulating local phenomena of CFD models make this approach optimal when wide-ranging results are requested. Moreover, CFD models may support remarkably the analysis of flow areas in which experimental data are challenging to acquire due to the needed extreme precision and sophisticated apparatus and data collection techniques. As an example, CFD models allow simulating cavitating flows, including the growth and implosion of bubbles containing liquid vapour (Kornet *et al.* 2017).

With this aim, the first step is to set up a CFD model suitable for simulating the flow through an orifice in steady-state conditions characterised by a low-Reynolds number. The reasons for such a methodological choice are two: (i) the crucial role of geometrical characteristics in CFD models suggests considering the orifices as the most straightforward partial blockage feature and (ii) the low-Reynolds number flow is an ideal pre-transient regime condition since it gives rise to safe conditions for the pipe: inasmuch with small overpressures to avoid damage to the conduits and contaminant intrusion, e.g., if there is a leak (Keramat *et al.* 2020).

A very crucial aspect concerns the identification of proper experimental data to use for checking the performance of the CFD model. It is worth noting that the achievement of such a task required special attention, since most of the laboratory experiments of the orifice steady-state behaviour provide only the value of the discharge coefficient. This is due to the fact that orifices are often used for measuring the discharge and as a less sophisticated device than pressure-reducing valves (Meniconi *et al.*

2017) for flow and pressure control (Malavasi & Messa 2011; Malavasi & Fenini 2020; La Rosa *et al.* 2021).

This paper aims at simulating the steady-state flow through an orifice for laminar condition by means of a 3D-CFD model and demonstrating the results by the comparison with experimental data available in the literature. The paper is organised as follows. Firstly, the pertinent experimental results used for checking the CFD model performance are presented. The CFD model is described with particular attention to the setup and convergence assessment phases. CFD results are compared with the selected experimental data. Successively, in the flow field analysis section, the refined CFD model is used for highlighting the main features of the flow through an orifice. Finally, the main conclusions are summarised concerning the use of CFD models within TTBTs for partial blockage detection and characterisation.

FLOW-THROUGH ORIFICES

Experimental studies

Flow-through orifices have been extensively studied. A large number of these studies, mainly experimental, focused on fully developed turbulent flows where the orifice discharge coefficient, C_d, is nearly independent on the Reynolds (Re) number, $Re = UD/\nu$, with U = mean flow velocity in the pipe, D = internal pipe diameter, and ν = kinematic viscosity. Several numerical and experimental studies analysed the flow-through orifices with a low-Re number (Johansen 1930; Filban & Griffin 1960; Marxman & Burlage 1961; Zampaglione 1969; Keith & John 1977; Alvi *et al.* 1978; Phares *et al.* 2005; Jankowski *et al.* 2008). Within such a vast body of literature, only the most relevant papers, whose experimental data are used in the present analysis, are referred to herein.

According to the literature (e.g., Tu *et al.* 2006) any feature, Φ, characterising the flow through an orifice (Figure 2) can be expressed by means of the following dimensionless relationship:

$$\Phi = f(\phi, \beta, Eu, Re) \quad (1)$$

where ϕ is the length-to-diameter ratio ($= L/d$), β is the diameter ratio ($= d/D$), and Eu is the Euler number

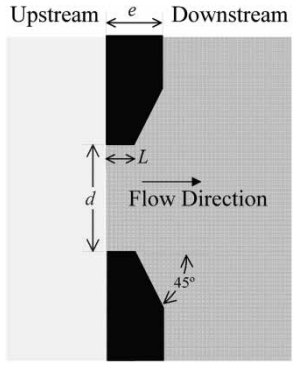

Figure 2 | Orifice detail schematics.

($= g\Delta H/U^2$), with L = length of the orifice in the flow direction (Figure 2), d = orifice diameter, g = gravity acceleration, and ΔH = local head loss through the orifice.

According to the value of ϕ, orifices can be classified into: (i) thin-walled or sharp-edged orifices for $\phi \leq 0.125$; (ii) thick-walled orifices for $0.125 < \phi < 2$ and (iii) short tube or orifice tube for $\phi \geq 2$. In this paper, a sharp-edged orifice with $L = 0$, centred at the pipe axis, introduced in a plate with a thickness $e = 1$ mm, bevelled at 45° at the outlet (downstream), is considered. This choice is justified by the fact that, for such a layout, experimental data are available at the required flow regime (i.e., small values of Re). Below some information about selected experimental studies are reported.

Johansen (1930) carried out extensive series of experimental tests on a concentric sharp-edged orifice for a range of low-Re numbers (from 222 to 1,020), considering four diameter ratios, β =0.209, 0.401, 0.595 and 0.794. Later, these results have been considered by Jankowski *et al.* (2008), who developed a semi-empirical model for estimating the discharge coefficient, C_d, for flow-through sharp-edged orifices.

Zampaglione (1969) carried out an accurate experimental analysis about the flow through a sharp-edged orifice for five diameter ratios, $\beta = 0.214$, 0.319, 0.425, 0.575 and 0.697. For each β value, the analysed flow range, defined on the basis of Re, was limited to stable laminar conditions, i.e., with no pulsating flow. In his experiments, Zampaglione (1969) pointed out that for Re smaller than a critical value, Re_{crit}, no pulsating phenomena occurred. Later, Alvi *et al.* (1978) run laboratory tests for sharp-edged orifices taking

into account data from Zampaglione (1969) and Rao & Sridharan (1972).

As mentioned, the parameter globally describing the flow through an orifice is the flow discharge coefficient, C_d:

$$C_d = \frac{Q}{A\beta^2}\sqrt{\frac{(1-\beta^4)}{2g\Delta H}} \tag{2}$$

in which Q is the discharge and A is the cross-section area of the pipe. It is important to highlight that the local head loss, ΔH, completes (Figure 3) at a distance downstream of the orifice equal to the length of the expansion cone, X^*, where the flow re-attaches the pipe wall.

Jankowski *et al.* (2008) developed a semi-empirical formulation, based on experimental data from the literature, that gives an approximation, $C_{d,s}$, of the exact value of the discharge coefficient:

$$C_{d,s} = 0.6\left[1 + \exp\left(-0.12\sqrt{\frac{Re}{\beta}}\right) - 2.16\exp\left(-0.26\sqrt{\frac{Re}{\beta}}\right) + 0.16\left(1 - \frac{\sqrt{\frac{Re}{\beta}}}{1+\sqrt{\frac{Re}{\beta}}}\right)\right] \tag{3}$$

which is valid for flow-through sharp-edged orifices, $\phi = 0$, and small diameter ratios ($\beta \leq 0.25$).

For characterising an orifice, as an alternative to C_d, the flow coefficient, Λ, has been proposed by Zampaglione (1969):

$$\Lambda = \frac{Q}{A_d\sqrt{2g\Delta H_{max}}} \tag{4}$$

where ΔH_{max} is the pressure head difference between two points: the one immediately upstream of the orifice and the other one immediately downstream of it (Figure 3), where the minimum value of the pressure head occurs, and A_d is the cross-sectional area of the orifice. It is worth noting that ΔH and ΔH_{max} focus the attention on the head loss and pressure decrease through the orifice, respectively. As a consequence, the combination of ΔH and ΔH_{max} allows properly describing the behaviour of the flow through the orifice.

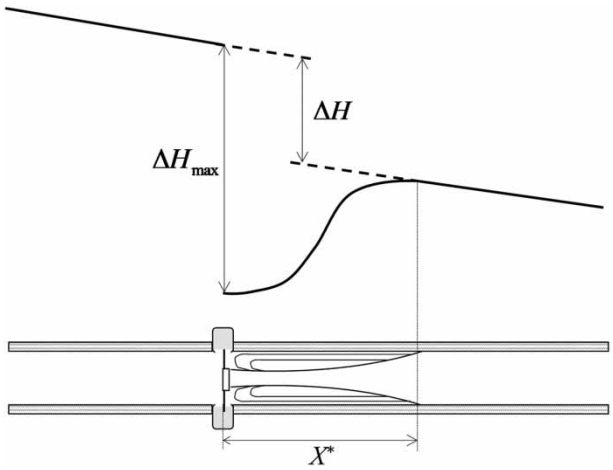

Figure 3 | Pressure decrease, ΔH_{max}, and local head loss, ΔH, through an orifice, with X^* being the length of the expansion cone (schematic).

CFD MODEL DEVELOPMENT

Governing equations

In CFD models, the governing equations are derived from the conservation principles of mass and momentum. The principle of mass conservation for a compressible fluid (Fay 1994; Krepper *et al.* 2009) indicates that, in the absence of mass sources and sinks, a region will conserve its mass on a local level and is described by the continuity equation:

$$\frac{D\rho}{Dt} + \rho\frac{\partial u_k}{\partial x_k} = 0 \tag{5}$$

where t is the time, ρ is the fluid density and u_k is the velocity component in the spatial coordinate x_k (with k =1, 2, 3).

The momentum conservation principle indicates that the momentum time variation equals the summation of the external forces (Bird *et al.* 2002). This principle expressed in terms of the Cauchy stress tensor, σ, is known as the Cauchy equations:

$$\rho\frac{Du_i}{Dt} = \frac{\partial \sigma_{ij}}{\partial x_j} + \rho f_i \tag{6}$$

where f represents the mass forces per unit mass acting on the fluid (i.e., gravity).

The constitutive equations of the fluid relate the stress tensor to the velocity gradients, describing the rheological behaviour of the fluid. The constitutive equations of the stress tensor for isotropic, homogenous and Newtonian fluids are:

$$\sigma_{ij} = -p\delta_{ij} + \lambda\delta_{ij}\frac{\partial u_k}{\partial x_k} + \mu\left(\frac{\partial u_i}{\partial x_j} + \frac{\partial u_j}{\partial x_i}\right) \tag{7}$$

where p is the thermodynamic pressure, δ_{ij} is the Kronecker function, μ is the dynamic viscosity and λ is the second viscosity ($\lambda = -2/3\mu$). Inserting the stress–strain law given by Equation (7) in the momentum equation yields the general form of the Navier–Stokes (N–S) equations for isotropic and Newtonian fluids:

$$\rho\frac{Du_i}{Dt} = \rho f_i - \frac{\partial p}{\partial x_i} - \frac{\partial}{\partial x_i}\left(\lambda\frac{\partial u_k}{\partial x_k}\right) + \frac{\partial}{\partial x_j}\left[\mu\left(\frac{\partial u_i}{\partial x_j} + \frac{\partial u_j}{\partial x_i}\right)\right] \tag{8}$$

To close the problem, it is necessary to specify the initial and boundary conditions in space and time (Denton & Dawes 1998).

Model setup

CFD simulations are carried out using an open-source software, OpenFOAM, which is divided into two key phases: the pre-processing and the simulation stage.

The pre-processing stage includes the definition of the fluid domain, mesh generation and model setup, as well as the definition of boundaries and solver parameters.

As a mesh generation tool, the snappyHexMesh (OpenFOAM built-in) is used. This tool considers a basic mesh (generated in blockMesh – OpenFOAM built-in) and the shape of the chosen geometry defined in a computer-aided design software. Then, the generated cuboid mesh is sculpted and refined, adjusting it to the chosen geometry. In the simulations below, a 4-m cylindrical shape (pipe) with D =0.02 m with a concentric orifice, with a e =1 mm thick plate positioned in the middle of the pipe length (Figure 4), is considered. Within mesh generation, the initial cuboid mesh is refined in three directions considering the mesh parameters proposed by Martins et al. (2014): $\eta_a = 0.57$, $\eta_c = 0.009$ and $\eta_r = 0.03$, in which the subscripts of the mesh parameter η, a, c and r stand for axial, circumferential and radial directions, respectively. Accordingly, three meshes were obtained, one for each of the considered diameter ratio, β (=0.214, 0.425 and 0.697) characterised by 7.8, 8.4 and 8.9 million cells and 11.2, 12 and 12.4 million points, respectively. The generated meshes present a minimum and a maximum volume equal to 8.1×10^{-15} and 2.6×10^{-8}m^3, respectively. With respect to the previous work of Martins et al. (2014), where the high-velocity gradients were expected strictly on the walls, the mesh considered herein presents a much larger number of cells with the mesh refinements not only close to the orifice and in the corners between the pipe and the plate, but also in the whole flow domain. This is a necessary premise to the subsequent simulation that will be carried out in transient conditions. In fact, even if the upstream flow is laminar, the behaviour of the flow downstream of the orifice is much more complex, with the orifice leading to flow contraction and detachment and creating large circumferential eddies. This suggests the need for the above-mentioned extra mesh refinements in anticipation of the interaction with sharp pressure waves, such as those generated during transients for fault detection.

Note that the radial mesh parameter, η_r, i.e., the location of the first point away from the pipe wall, is larger than the one proposed by Martins et al. (2014) for Re = 1,394. Since

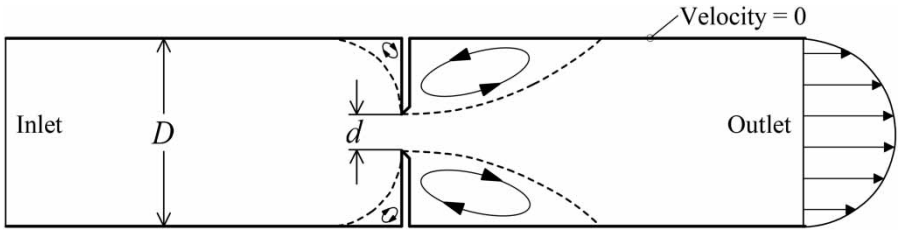

Figure 4 | Setup configuration.

this analysis focuses on $Re < 350$, the considered η_r was 0.03; however, to confirm that the η_r does not affect the accuracy of this specific solution, values of $\eta_r < 0.03$ were analysed but for the sake of brevity not presented herein. Such values of η_r result in meshes up to 30 million cells, three times larger than the used ones, but with the same accuracy.

As a final result of the pre-processing stage, the fluid domain has been divided into smaller, non-overlapping subdomains generating a mesh of cells with Equations (5) and (6) numerically solved in each of them.

Appropriate boundary conditions are considered (Figure 4): the velocity defines the flow at the outlet, the pressure the one at the inlet and is assumed the no-slip condition at the pipe wall.

In the second stage, CFD simulations are run for the laminar flow in steady-state conditions. In OpenFOAM, the N–S and continuity equations are resolved by the rhoSimpleFOAM solver based on the finite volume method. RhoSimpleFOAM is a pressure-based solver considering the relationship between pressure and velocity adjustments to carry out the mass conservation to obtain the pressure field.

The convergence of the numerical solution can be assessed by progressively tracking the imbalances accentuated by the advancing numerical calculations of the algebraic equations through each iteration. This imbalance, usually referred to as *residuals*, measures the overall conservation of the flow properties. The solution is assumed to have converged when the *residuals* value drops below 10^{-7}.

SIMULATED SCENARIOS

CFD simulations were carried out for three sharp-edged orifices ($\phi = L/d = 0$) with a diameter ratio $\beta(= d/D)$ equal to 0.214, 0.425 and 0.697. Such values match the smallest, median and largest values of β, analysed by Zampaglione (1969). In the numerical experiments, Re ranges between 1 and 350 and, for each β, the maximum value of Re is smaller than the critical value, Re_{crit}. Precisely, $120 < Re_{crit} < 130$ for $\beta = 0.214$, $250 < Re_{crit} < 300$ for $\beta = 0.425$, and $350 < Re_{crit} < 400$ for $\beta = 0.697$. For the smallest $\beta(= 0.214)$, a set of 18 simulations were run, each for a different value of Re (i.e., 1, 2, 3, 4, 6, 8, 10, 20, 30, 40, 50, 60, 70, 80, 90, 100, 110, and 120). For $\beta = 0.425$, simulations were run for five Re (i.e., 130, 140, 150, 200 and 250) beyond the ones that were considered for $\beta = 0.214$. For $\beta = 0.697$, the CFD model was run for the same values of Re as for $\beta = 0.425$ and two more (i.e., 300 and 350).

COMPARISON WITH EXPERIMENTAL DATA

As mentioned, Zampaglione (1969) and Johansen (1930) carried out laboratory tests for capturing the main features of a laminar flow through an orifice. The CFD numerical and the experimental results obtained for the largest and smallest diameter ratios by the previous authors with regard to Λ and C_d values are plotted in Figure 5.

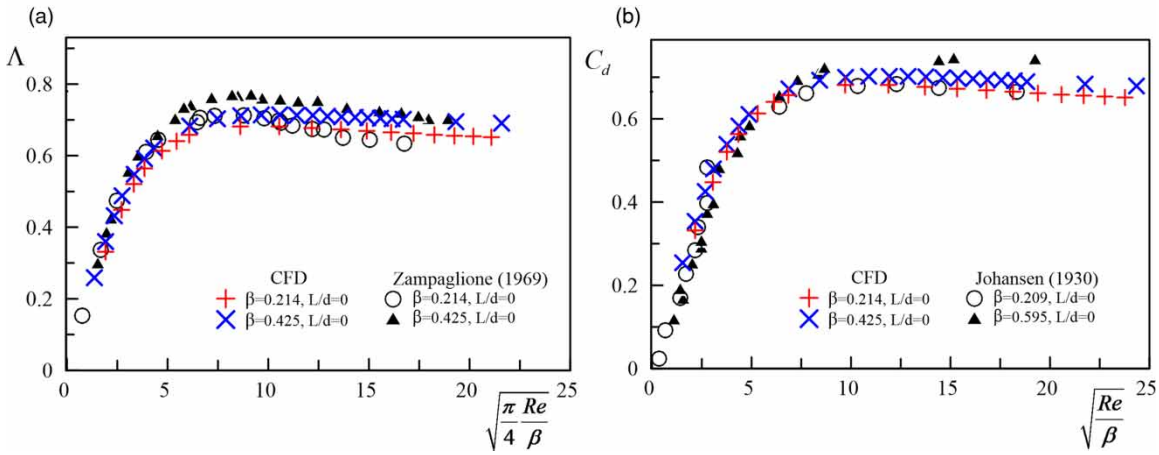

Figure 5 | CFD results vs. experimental data from (a) Zampaglione (1969) and (b) Johansen (1930).

Numerical results have an excellent agreement with experimental data. The small differences observed in Figure 5(b) are due to the fact that experimental data from Johansen (1930) correspond to slightly different diameter ratios. Precisely, CFD data correspond to $\beta = 0.214$ and 0.425, whereas the Johansen (1930) ones correspond to $\beta = 0.209$ and 0.595.

The semi-empirical values of C_d by Jankowski *et al.* (2008) are compared with those given by CFD in Figure 6. The numerical results fit very well the experimental data as well as with the semi-empirical Equation (3) valid for $\beta \leq 0.25$ by Jankowski *et al.* (2008). It is worth noting a slightly better match with the experimental data from Johansen (1930).

The comparison of the CFD results with the Alvi *et al.* (1978) and Zampaglione (1969) experimental data in terms of *Eu* values is depicted in Figure 7. CFD results are in good agreement with those by Zampaglione (1969). Despite Alvi *et al.* (1978) experimental data, represented by the dashed lines, corresponding to a different diameter ratio,

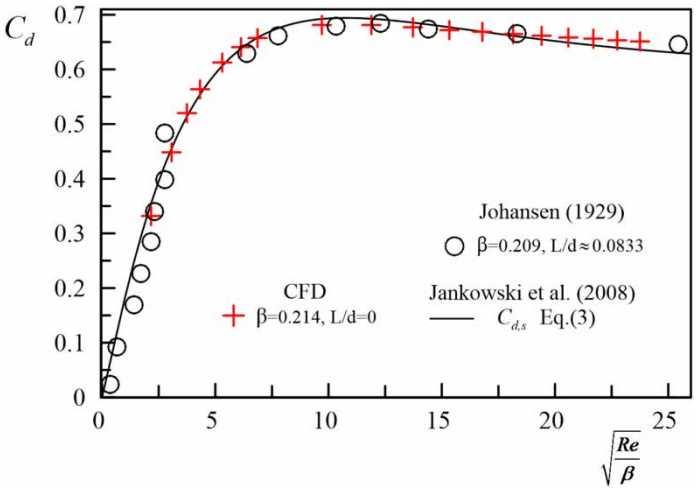

Figure 6 | C_d values based on the experimental data by Johansen (1930) and semi-empirical results by Jankowski *et al.* (2008) vs. CFD results.

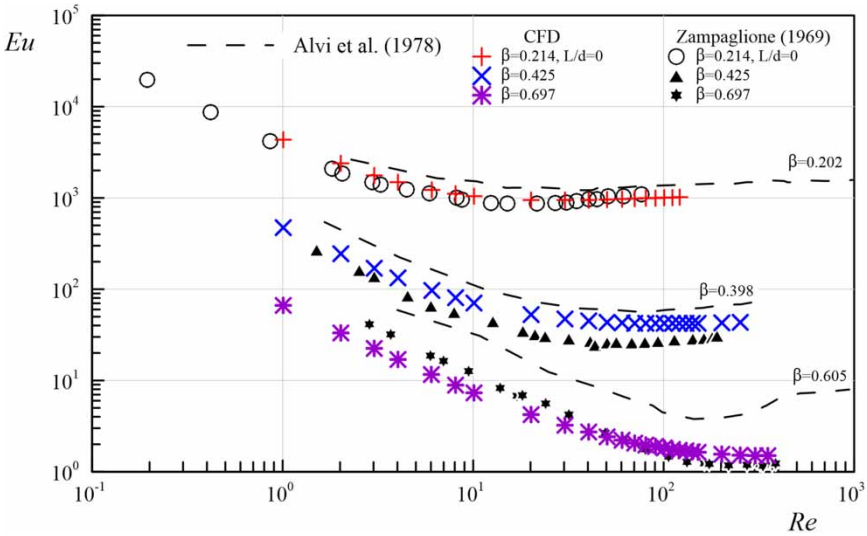

Figure 7 | *Eu* values based on experimental data by Zampaglione (1969) and Alvi *et al.* (1978) vs. CFD results.

β, with respect to CFD and the Zampaglione (1969) data, the trends are alike and follow the same behaviour.

The CFD results in terms of the length of the expansion cone, X^*, are in accordance with those obtained experimentally by Zampaglione (1969), as shown in Figure 8. In this figure, the results are represented by means of two dimensionless parameters: the relative length, $x^* = X^*/D$, and *Re*, where $X^* = x_{tl} - x_d$, with x_{tl} = coordinate along the axis (centreline) where contracted region re-attaches the wall (the subscript 'tl' indicates the total length), and $x_d$is the location of the orifice (Figure 3). It is worth noting that the characteristics of the expansion cone – in Italian *corrente viva* (Russo Spena 1951) – could play an important role during transients with regard to the mechanisms of interaction with pressure waves.

FLOW FIELD ANALYSIS

In the light of the above positive results of the comparison between experimental and CFD results, in this section, the characteristics of the flow field immediately upstream and downstream of the orifice are analysed by means of the CFD model. As mentioned, such a detailed picture of the flow field around the orifice will surely help in the analysis of the interaction with pressure waves in transient conditions.

The presence of an obstacle, represented herein by a plate with a concentric orifice, requires the flow to contract to the core and separate from the walls (Figure 9). Upstream of the orifice, the flow separates from the walls, leaving a circumferential void, where a swirl (eddy) forms between the separation zone and the orifice plate (Mills 2006). In the contracted region, high velocities occur in the core, increasing with *Re*. Downstream of the orifice, around the contracted core region (*corrente viva*), a swirl of fluid happens, with velocity components towards the orifice and away from it, contributing to the local head loss. In other words, the existence of an obstacle generates two eddies around the *corrente viva*, located upstream and downstream of the orifice plate (Figure 9), symmetrical for the particular case of the 'creeping flow'. Precisely, such a flow occurs when fluid velocities are very small and, as a consequence, inertial forces are small compared with the viscous ones (Bird *et al.* 2002; White 2003; Çengel & Cimbala 2014). Figure 9 points out that, as *Re* increases, the downstream eddy elongates in the flow direction, while the upstream eddy decreases in size and becomes almost imperceptible (Mills 2006). The eddy elongation, increasing with *Re*, also occurs in many other physical phenomena, such as the external flow around the spheres and cylinders (Rocha *et al.* 2007).

The observed eddies that are not part of the *corrente viva* hardly contribute to the discharge since most of the velocities cancel each other. These eddies imply flow recirculation, contributing to the local head loss by extracting momentum from the *corrente viva*. Such a behaviour

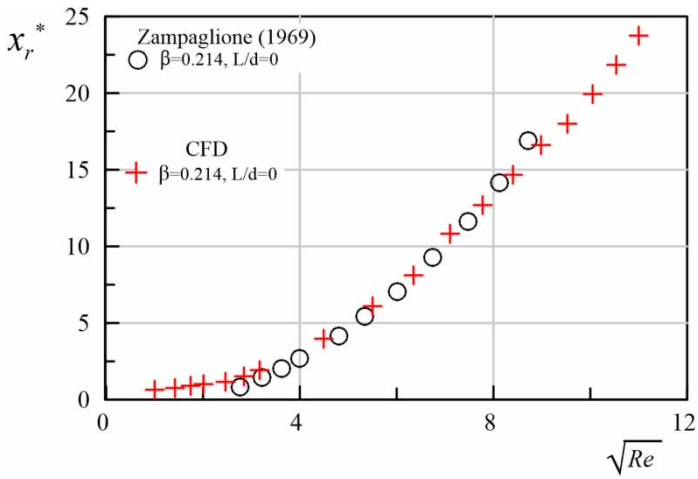

Figure 8 | Relative length of the expansion cone as a function of *Re* by Zampaglione (1969) vs. CFD results.

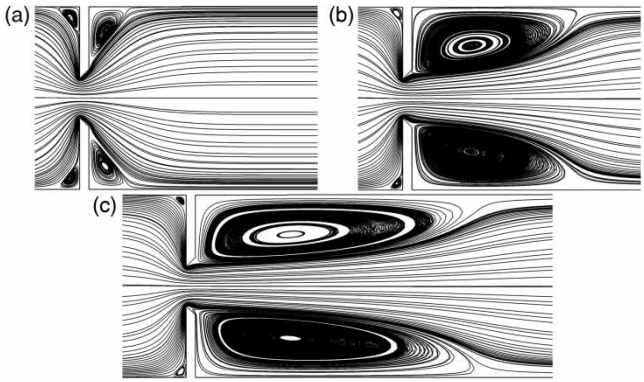

Figure 9 | CFD streamlines for $\beta = 0.214$: (a) $Re = 1$, (b) $Re = 6$ and (c) $Re = 10$.

confirms the quantitative observations by Zampaglione (1969) about the progressive increase of the size of the eddies with Re, even in the laminar flow regime.

The head, H, calculated by the CFD model, for $\beta = 0.214$, and for a range of Re between 1 and smaller than Re_{crit}, is presented in Figure 10 in terms of two dimensionless parameters: the relative length, x^*, and $H^* = (H - H_0)/\Delta H$, where subscript 0 refers the quantity to the section at the 'inlet', immediately upstream of the orifice. In Figure 9, markers '+' indicate the relative length of the expansion cone. The expansion cone and the re-attachment can be observed in Figure 11, where the *corrente viva* is plotted. These curves show that,

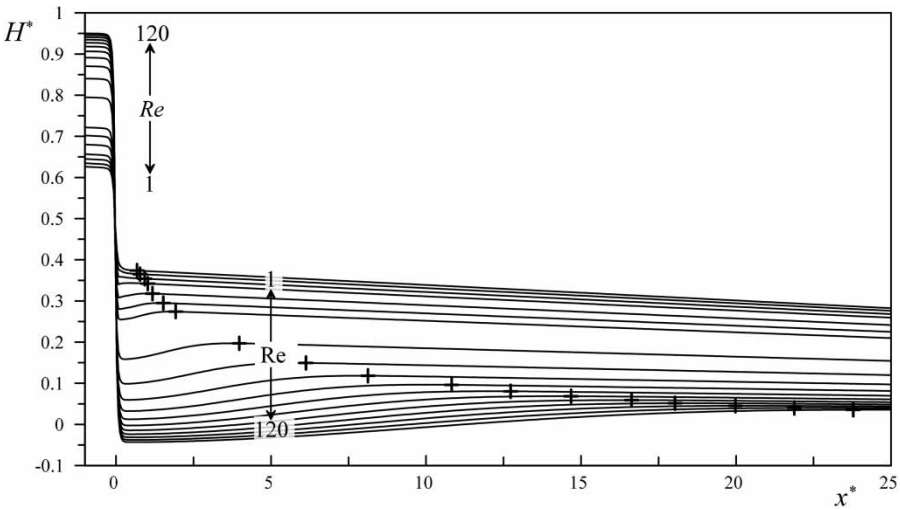

Figure 10 | Dimensionless pressure head, H^*, for $\beta = 0.214$ ('+' marker indicates the relative length of the expansion cone).

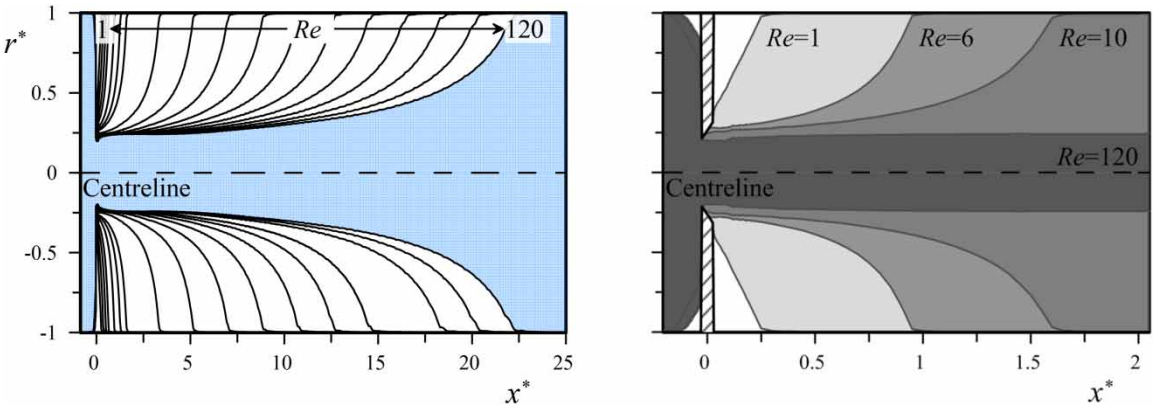

Figure 11 | Streamline envelops of *corrente viva* for the diameter ratio $\beta = 0.214$ for: (a) $1 \leq Re \leq 120$ and (b) magnified vision for $Re = 1$, 6, 10 and 120.

downstream of the orifice, the expansion cone enlarges progressively, in different ratios associated with *Re*, and re-attaches at a downstream point, highlighted by the markers '+' in Figure 10. Outside the expansion cone, and while the flow region surrounding the *corrente viva* decreases, the flow decelerates until the re-attachment occurs.

Figure 11(a) shows the full range of *Re* of the expansion cones analysed for $\beta = 0.214$, whereas in Figure 11(b) a magnified vision of the expansion cone is reported, only for four values of *Re* (1, 6 and 10, and the maximum considered $Re = 120$); in this figure, $r^* = r/R$, with r = distance from the axis and R = pipe radius. The presented envelops of the *corrente viva* (Figure 11(b)) show that for small *Re*, such a feature is attached to the downstream bevelled surface of the orifice, while for $Re = 120$, the flow separates at the upstream tip of the orifice. Figure 11 also shows that, as *Re* increases, the separated flow region, where eddies are located, extends downstream, occupying a larger pipe extension.

Figure 12 shows the evolution of the velocity flow field close to the orifice, represented by the velocity profiles, for four values of *Re* (1, 6, 10 and 120) and four distances both upstream and downstream of the orifice; in this figure, the dimensionless velocity, $u^* = u/u_d$, is used, with u_d = velocity at the orifice axis.

In the first row of Figure 12, corresponding to $Re = 1$, it can be observed that the velocity fields, both upstream and downstream of the orifice, are close to being symmetrical since *Re* is small and closer to the 'creeping flow'. As *Re* increases, the downstream velocity field evolves, presenting a substantially different behaviour. Precisely, for $Re = 6$ and 10, the velocity profiles show that the maximum velocity occurs very close to the orifice, i.e., at $0 < x^* < 0.05$. A different behaviour is observed for $Re = 120$, where the maximum value occurs beyond $x^* > 0.10$, and the velocity in the axis is increasing in $0.05 < x^* < 0.10$. Moreover, a characteristic behaviour can be observed in the shape of the velocity profile in the orifice, indicated by means of a grey line. Precisely, for $Re \leq 6$, the shape of the velocity profiles is rounded and elongated, whereas for higher *Re* (i.e., >10), the velocity profile takes a squared shape, even more pronounced for $Re = 120$. This means that, as the discharge increases, velocity distribution tends to a constant profile, typically of rapidly accelerated flows. In addition, for $Re = 120$ at $x^* = 0.10$, it can be observed that the maximum velocity in the orifice section does not occur at the axis but close to the walls, as observed in Kashi *et al.* (2018). It is worth mentioning that such a different behaviour, in steady-state conditions, could reflect in a different mechanism of interaction with the incoming pressure waves.

CONCLUSIONS

The narrowing of the pipe cross-section (partial blockage) can cause severe impacts on pipe system hydraulic performance by reducing the transport capacity in gravity systems and increasing the local head losses and then the energy consumption and associated operating costs in rising systems. The partial blockages can also deteriorate the water quality by allowing the growth of the biofilm. Such features can be avoided if partial blockages are detected at an early stage of the development.

Literature on TTBTs shows that the transient response of a pipe with a partial blockage is quite different from the one of the corresponding defect-free pipe. Such differences depend on the location and severity of the blockage. However, within TTBTs, the 1D approaches do not allow the characteristics of the blockage to be evaluated with a good precision. In fact, within 1D models, only the local head loss through the orifice can be considered. In the writers' opinion, to improve the performance of TTBTs, more complete models must be considered. This justifies the interest in CFD models that can include more detailed information about the characteristics of the flow field.

In this paper, the flow through a sharp-edged orifice for different sizes and values of the Reynolds number, *Re*, is simulated by means of a CFD model developed in OpenFOAM. Numerical results show excellent agreement with the experimental data available in the literature.

The good performance of the CFD model in terms of both global and local quantities, authorised exploring in detail the features of the flow around the orifice, which depend on *Re*. The analysis focused on the contracted core region (*corrente viva*) downstream of the orifice, the upstream and downstream eddies responsible for the momentum dissipation, and the elongation of the

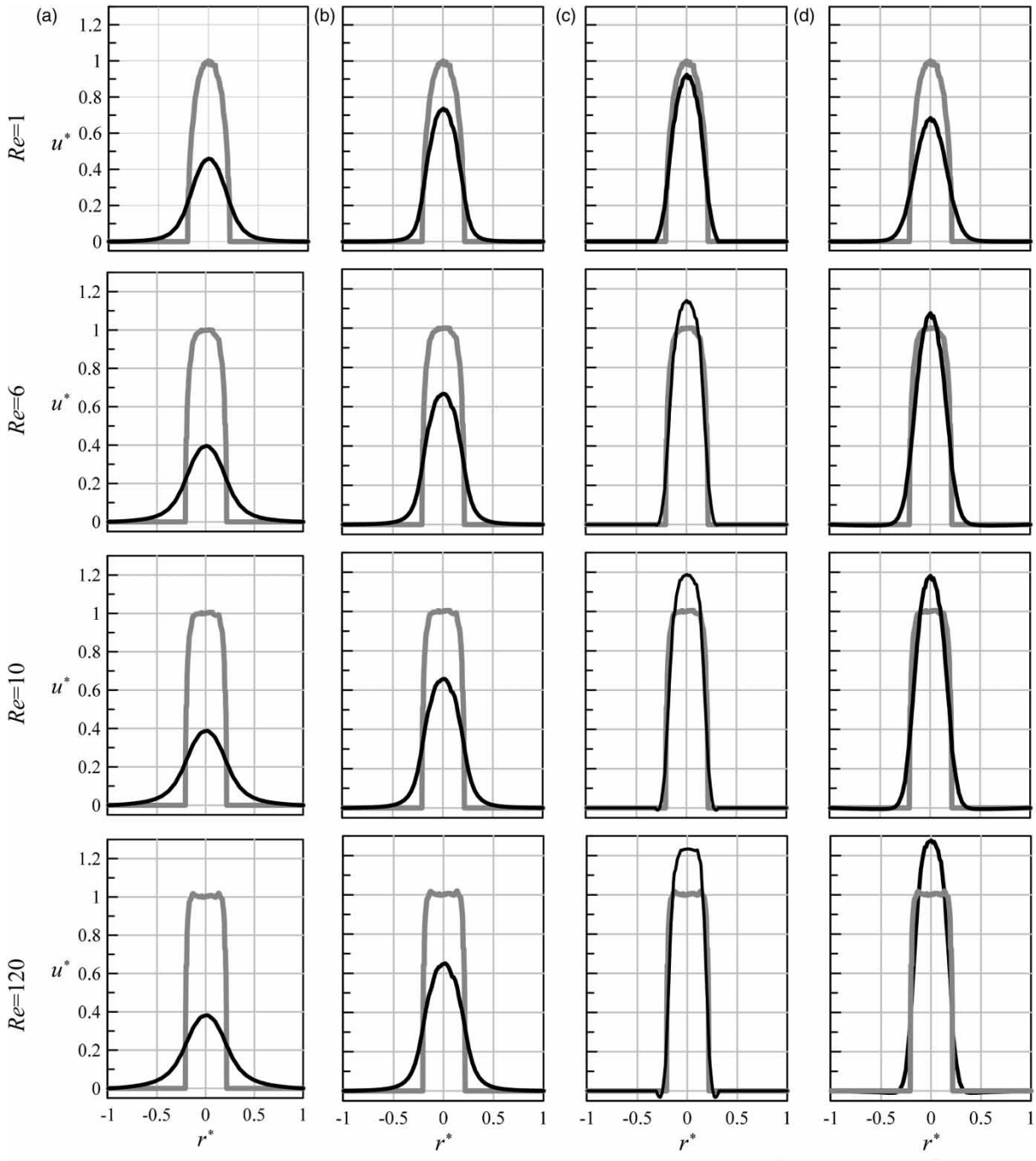

Figure 12 | Velocity profiles for diameter ratio $\beta = 0.214$, ——— at the orifice ($x^* = 0$) (a) $x^* = -0.10$; (b) $x^* = -0.05$; (c) $x^* = 0.05$ and (d) $x^* = 0.10$.

downstream eddy. The CFD simulations have allowed a better understanding of the Reynolds number-dependent features of the flow around the orifice, which had never been experimentally nor numerically observed before. It should be highlighted that the experimental observation of those features is only possible to visualise with such detail by using state-of-the-art and very expensive instrumentation (e.g. Laser Doppler Velocimetry or Particle Image

Velocimetry techniques). In fact, these features can play an important role in the mechanisms of interaction with the pressure waves during transient tests for the orifice characterisation.

The paper demonstrates that the CFD model is capable of simulating the steady-state flow through a sharp-edged orifice for low-Reynolds number, by the excellent agreement obtained between the numerical results and the experimental data available in the literature. The paper is the first step forward to using CFD models to detect partial blockages (pipe cross-section reduction) in pipes. The next step is to use these CFD models to simulate transient-state conditions in pipes with intermediate blockages and to analyse reflected pressure waves as a function of the blockage size and location.

ACKNOWLEDGEMENTS

The authors would like to thank the Fundação para a Ciência e Tecnologia for funding the Project PTDC/ECI-EGC/32102/2017, iMIST – Improving Mixing in Storage Tanks for Safer Water Supply and the Hong Kong (HK) Research Grant Council Theme-Based Research Scheme and the HK University of Science and Technology (HKUST) under the project 'Smart Urban Water Supply System (Smart UWSS)'.

DATA AVAILABILITY STATEMENT

All relevant data are included in the paper or its Supplementary Information.

REFERENCES

Alegre, H. & Covas, D. 2010 *Gestão Patrimonial de Infra-Estruturas de Abastecimento de Água: Uma Abordagem Centrada na Reabilitação (in Portuguese)*. ERSAR, LNEC, IST, Lisboa.

Alvi, S. H., Sridharan, K. & Rao, N. S. L. 1978 Loss characteristics of orifices and nozzles. *Journal of Fluids Engineering-Transactions of the ASME* **100**, 299–307. doi:10.1115/1.3448670.

Bach, R. G. & Kern, M. J. 1997 Clinical application of the Doppler flow velocity guide wire. *Cardiology Clinics* **15**, 77–99. doi:10.1016/s0733-8651(05)70320-9.

Badillo-Olvera, A., Pérez-González, A., Begovich, O. & Ruíz-León, J. 2019 Burst detection and localization in water pipelines based on an extended differential evolution algorithm. *Journal of Hydroinformatics*. doi:10.2166/hydro.2019.123.

Beck, S. B. M., Collins, R. P., Meruane, V., Meyers, G. & Butterfield, J. D. 2018 Experimental investigation into techniques to predict leak shapes in water distribution systems using vibration measurements. *Journal of Hydroinformatics* **20**, 815–828. doi:10.2166/hydro.2018.117.

Bird, R. B., Stewart, W. E. & Lightfoot, E. N. 2002 *Transport Phenomena*. John Wiley & Sons, Inc, New York.

Çengel, Y. A. & Cimbala, J. M. 2014 *Fluid Mechanics-Fundamentals and Applications*, 3rd edn. McGraw Hill, New York.

Chaudhry, M. H. 2014 *Applied Hydraulic Transients*, 3rd edn. Springer-Verlag, New York. doi:10.1007/978-1-4614-8538-4.

Contractor, D. N. 1965 The reflection of waterhammer pressure waves from minor losses. *Journal of Basic Engineering* **87**, 445–451.

Denton, J. D. & Dawes, W. N. 1998 Computational fluid dynamics for turbomachinery design. *Proceedings of the Institution of Mechanical Engineers, Part C: Journal of Mechanical Engineering Science* **213**, 107–124.

Duan, H.-F. 2017 Transient frequency response based leak detection in water supply pipeline systems with branched and looped junctions. *Journal of Hydroinformatics* **19**, 17–30. doi:10.2166/hydro.2016.008.

Duan, H.-F., Wang, R. & Sun, J. 2016 Multiple-fault detection in water pipelines using transient-based time-frequency analysis. *Journal of Hydroinformatics* **18**, 975–989. doi:10.2166/hydro.2016.232.

Fay, J. A. 1994 *Introduction to Fluid Mechanics*. MIT Press, Cambridge, MA.

Ferrante, M., Brunone, B., Meniconi, S., Karney, B. W. & Massari, C. 2014 Leak size, detectability and test conditions in pressurized pipe systems. *Water Resources Management* **28**, 4583–4598. doi:10.1007/s11269-014-0752-6.

Ferreira, J. P., Buttarazzi, N., Ferras, D. & Covas, D. I. C. 2020 Effect of entrapped air on hydraulic transients in pressurized pipes. *Journal of Hydraulic Research* 1–13. doi:10.1080/00221686.2020.1862323.

Filban, T. J. & Griffin, W. A. 1960 Small-diameter-orifice metering. *Journal of Basic Engineering* **82**, 735–738. doi:10.1115/1.3662729.

Gong, J., Lambert, M. F., Simpson, A. R. & Zecchin, A. C. 2014 Detection of localized deterioration distributed along single pipelines by reconstructive MOC analysis. *Journal of Hydraulic Engineering* **140**, 190–198. doi:10.1061/(asce)hy.1943-7900.0000806.

Gooch, R. M., Clarke, T. A. & Ellis, T. J. 1996 A semi-autonomous sewer surveillance and inspection vehicle. In *Conference on*

Intelligent Vehicles, Tokyo, Japan, pp. 64–69. doi:10.1109/IVS.1996.566354.

Jankowski, T. A., Schmierer, E. N., Prenger, F. C. & Ashworth, S. P. 2008 A series pressure drop representation for flow through orifice tubes. *Journal of Fluids Engineering-Transactions of the ASME* **130**. doi:10.1115/1.2907408.

Jing, L., Li, Z., Wang, W., Dubey, A., Lee, P., Meniconi, S., Brunone, B. & Murch, R. D. 2018 An approximate inverse scattering technique for reconstructing blockage profiles in water pipelines using acoustic transients. *Journal of the Acoustical Society of America* **143**, EL322. doi:10.1121/1.5036957.

Johansen, F. C. 1930 Flow through pipe orifices at low reynolds numbers. *Proceedings of the Royal Society A: Mathematical, Physical and Engineering Sciences* **126**, 231–245. doi:10.1098/rspa.1930.0004.

Kashi, B., Weinberg, E. & Haustein, H. D. 2018 Analytial re-examination of the submerged laminar jet's velocity evolution. *Physics of Fluids* **30**. doi:10.1063/1.5028560.

Keith, T. G. & John, J. E. A. 1977 Calculated orifice plate discharge coefficients at low reynolds numbers. *Journal of Fluids Engineering* **99**, 424–425.

Keramat, A., Payesteh, M., Brunone, B. & Meniconi, S. 2020 Interdependence of flow and system characteristics in transient induced contamination intrusion in pipes: numerical analysis. *Journal of Hydroinformatics*. doi:10.2166/hydro.2020.069.

Kornet, S., Lipiński, S. & Niedźwiedzka, A. 2017 Verification of CFD tool for simulation of cavitating flows in hydraulic systems. *Journal of Hydroinformatics* **19**, 653–665. doi:10.2166/hydro.2017.004.

Krepper, E., Cartland-Glover, G. & Grahn, A. 2009 CFD modelling of insulation debris transport phenomena in water flow. *Kerntechnik* **74**, 255–264.

La Rosa, D. M., Rossi, M. M. A., Ferrarese, G. & Malavasi, S. 2021 On the pressure losses through multistage perforated plates. *Journal of Fluids Engineering* **143**. doi:10.1115/1.4049937.

Li, J., Wu, Y. & Lu, C. 2020 Pipeline leak detection using the multiple signal classification-like method. *Journal of Hydroinformatics* **22**, 1321–1337. doi:10.2166/hydro.2020.194.

Louati, M., Meniconi, S., Ghidaoui, M. S. & Brunone, B. 2017 Experimental study of the eigenfrequency shift mechanism in a blocked pipe system. *Journal of Hydraulic Engineering* **143**, 04017044. doi:10.1061/(asce)hy.1943-7900.0001347.

Malavasi, S. & Fenini, L. 2020 Prediction of flow-control devices' noise with modified acoustic perturbation equations. *Journal of Hydroinformatics* **22**, 619–627. doi:10.2166/hydro.2020.156.

Malavasi, S. & Messa, G. V. 2011 Dissipation and cavitation characteristics of single-hole orifices. *Journal of Fluids Engineering* **133**. doi:10.1115/1.4004038.

Martins, N. M. C., Carriço, N. J. G., Ramos, H. M. & Covas, D. I. C. 2014 Velocity-distribution in pressurized pipe flow using CFD: accuracy and mesh analysis. *Computational Fluids* **105**, 218–230. doi:10.1016/j.compfluid.2014.09.031.

Marxman, G. A. & Burlage, J. H. 1961 Expansion coefficients for orifice meters in pipes less than one inch in diameter. *Journal of Basic Engineering* **83**, 289–298. doi:10.1115/1.3658945.

Massari, C., Yeh, T. C. J., Ferrante, M., Brunone, B. & Meniconi, S. 2014 Detection and sizing of extended partial blockages in pipelines by means of a stochastic successive linear estimator. *Journal of Hydroinformatics* **16**, 248. doi:10.2166/hydro.2013.172.

Meniconi, S., Brunone, B. & Ferrante, M. 2011a In-line pipe device checking by short-period analysis of transient tests. *Journal of Hydraulic Engineering* **137**, 713–722. doi:10.1061/(ASCE)Hy.1943-7900.0000309.

Meniconi, S., Brunone, B., Ferrante, M. & Massari, C. 2011b Small amplitude sharp pressure waves to diagnose pipe systems. *Water Resources Management* **25**, 79–96. doi:10.1007/s11269-010-9688-7.

Meniconi, S., Brunone, B., Ferrante, M. & Massari, C. 2011c Transient tests for locating and sizing illegal branches in pipe systems. *Journal of Hydroinformatics* **13**, 334–345. doi:10.2166/hydro.2011.012.

Meniconi, S., Brunone, B. & Ferrante, M. 2012a Water-hammer pressure waves interaction at cross-section changes in series in viscoelastic pipes. *Journal of Fluids and Structures* **33**, 44–58. doi:10.1016/j.jfluidstructs.2012.05.007.

Meniconi, S., Brunone, B., Ferrante, M. & Massari, C. 2012b Transient hydrodynamics of in-line valves in viscoelastic pressurized pipes: long-period analysis. *Experiments in Fluids* **53**, 265–275. doi:10.1007/s00348-012-1287-3.

Meniconi, S., Brunone, B., Ferrante, M., Capponi, C., Carrettini, C. A., Chiesa, C., Segalini, D. & Lanfranchi, E. A. 2015 Anomaly pre-localization in distribution-transmission mains by pump trip: preliminary field tests in the Milan pipe system. *Journal of Hydroinformatics* **17**, 377–389. doi:10.2166/hydro.2014.038.

Meniconi, S., Brunone, B., Ferrante, M. & Capponi, C. 2016 Mechanism of interaction of pressure waves at a discrete partial blockage. *Journal of Fluids and Structures* **62**, 33–45. doi:10.1016/j.jfluidstructs.2015.12.010.

Meniconi, S., Brunone, B., Mazzetti, E., Laucelli, D. B. & Borta, G. 2017 Hydraulic characterization and transient response of pressure reducing valves: laboratory experiments. *Journal of Hydroinformatics* **19**, jh2017158. doi:10.2166/hydro.2017.158.

Mills, R. D. 2006 Numerical solutions of viscous flow through a pipe orifice at low Reynolds numbers. *Journal of Mechanical Engineering Science* **10**, 133–140. doi:10.1243/jmes_jour_1968_010_020_02.

Mohapatra, P. K., Chaudhry, M. H., Kassem, A. A. & Moloo, J. 2006 Detection of partial blockage in single pipelines. *Journal of Hydraulic Engineering* **132**, 200–206.

Phares, D. J., Smedley, G. T. & Zhou, J. 2005 Laminar flow resistance in short microtubes international. *Journal of Heat and Fluid Flow* **26**, 506–512. doi:10.1016/j.ijheatfluidflow.2004.11.002.

Pozos-Estrada, O. 2018 Investigation of the combined effect of air pockets and air bubbles on fluid transients. *Journal of Hydroinformatics* **20**, 376–392. doi:10.2166/hydro.2017.018.

Quarteroni, A., Manzoni, A. & Vergara, C. 2017 The cardiovascular system: mathematical modelling, numerical

algorithms and clinical applicationsm. *Acta Numerica* **26**, 365–590. doi:10.1017/s0962492917000046.

Qunli, W. 1994 Reconstruction of blockage in a duct from single spectrum. *Applied Acoustics* **41**, 229–236. doi:10.1016/0003-682X(94)90073-6.

Qunli, W. & Fricke, F. 1989 Estimation of blockage dimensions in a duct using measured eigenfrequency shifts. *Journal of Sound and Vibration* **133**, 289–301. doi:10.1016/0022-460X(89)90927-9.

Rao, N. S. L. & Sridharan, K. 1972 Orifice losses for laminar approach flow. *Journal of the Hydraulics Division* **98**, 2015–2034.

Rocha, G. N., Poole, R. J. & Oliveira, P. J. 2007 Bifurcation phenomena in viscoelastic flows through a symmetric 1:4 expansion. *Journal of Non-Newtonian Fluid* **141**, 1–17. doi:10.1016/j.jnnfm.2006.08.008.

Rogers, L. M. 1995 Pipeline blockage location by strain measurement using a ROV. In *Offshore Technology Conference*, Houston, Texas. doi:10.4043/7862-MS.

Russo Spena, A. 1951 Contributo sperimentale allo studio dell'efflusso da tubi addizionali cilindrici. *Proc Accademia delle Scienze Fisiche e Matematiche Napoli* **4**, 1–35 (in Italian).

Soares, A. K., Covas, D. I. C. & Reis, L. F. R. 2011 Leak detection by inverse transient analysis in an experimental PVC pipe system. *Journal of Hydroinformatics* **13**, 153–166. doi:10.2166/hydro.2010.012.

Tu, X., Hrnjak, P. S. & Bullard, C. W. 2006 Refrigerant 134a liquid flow through micro-scale short tube orifices with/without phase change. *Experimental Thermal and Fluid Science* **30**, 253–262. doi:10.1016/j.expthermflusci.2005.07.004.

White, F. M. 2003 *Fluid Mechanics*, 5th edn. McGraw-Hill, New York.

Zampaglione, D. 1969 Sul moto di una corrente laminare attraverso diaframmi. *L'Energia Elettrica* **66**, 821–828.

Zouari, F., Louati, M., Meniconi, S., Blåsten, E., Ghidaoui, M. S. & Brunone, B. 2020 Experimental verification of the accuracy and robustness of area reconstruction method for pressurized water pipe system. *Journal of Hydraulic Engineering* **146**. doi:10.1061/(asce)hy.1943-7900.0001674.

First received 21 December 2020; accepted in revised form 19 April 2021. Available online 3 May 2021